X-ray Photoelectron Spectroscopy Equipped with Gas Cluster Ion Beams for Evaluation of the Sputtering Behavior of Various Nanomaterials

Hsun-Yun Chang,[†] Wei-Chun Lin,*,[†] Po-Chih Chu, Yi-Kai Wang, Mauo Sogo, Shin-ichi Iida, Chien-Jung Peng, and Takuya Miyayama*

Cite This: https://doi.org/10.1021/acsanm.2c00202
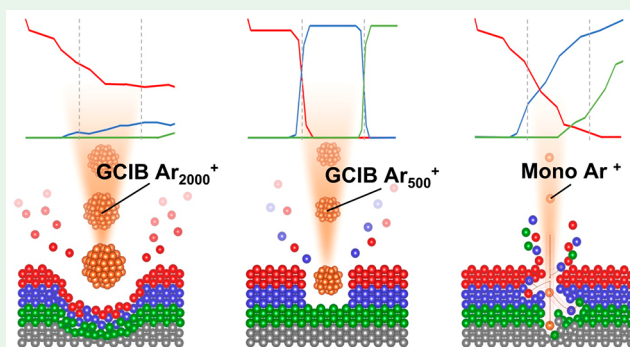
Read Online

ACCESS | Metrics & More | Article Recommendations | Supporting Information

ABSTRACT: The selection of ion-beam species and parameters for depth profiling requires experience to obtain accurate depth information and an efficient sputter rate on diverse samples. Sputter damage that causes changes in the chemical state and composition should be avoided. Monoatomic ion-beam sources are commonly utilized for the rapid sputtering of metals and inorganics, but sputter damage to highly oxidized metal oxides and organics is well-known. Cluster ion beams have become popular in recent years for soft materials because of their capability for low damage to organics, but sputter yields of metal and inorganic materials are very low. Currently, the material properties and structures of semiconductor devices have become more complicated because of rapid technical development. Thus, it is

necessary to explore more sputtering methods for samples with hybrid architecture that contain metals/inorganics/organics together. Recently, gas cluster ion beams (GCIBs) with small cluster sizes were considered to be one of the methods with the advantages of both monoatomic ion beams and conventional large-cluster GCIBs (>Ar_{2000}^+). A smaller-cluster GCIB results in higher energy per atom with a sputtering behavior similar to that of the monatomic ion beam and leads to enhancement of the sputter yield in metal and inorganic layers. However, the discussion of the cluster size selection for X-ray photoelectron spectroscopy (XPS) chemical state analysis during depth profiling is rather limited. In this work, a GCIB cluster measurement kit is developed and installed in an XPS system. The actual distribution of the cluster size of each GCIB setting can be measured before depth profiling. Depth profiling using GCIBs with a series of cluster sizes is performed to examine the sputter yield and evaluate the sputter effect on various organic, inorganic, and hybrid nanomaterials. The results also show the different sputtering behaviors of GCIBs with different cluster sizes ($Ar_{500-2000}^+$).

KEYWORDS: surface analysis, GCIB, controllable gas cluster, cluster size measurement, XPS, depth profiling, reduced sputter damage

1. INTRODUCTION

X-ray photoelectron spectroscopy (XPS) is one of the most commonly used surface analysis techniques to examine the surface composition and its chemical state.[1] Multiple ion beams are often provided on XPS systems as sputtering sources and used to remove thin layers of a few angstroms thick from the sample surface. When X-ray irradiation and ion-beam sputtering are alternately performed, nanoscale depth information may be ascertained.[2] The chemical state analysis and composition quantification within a nanoscale thin layer is then disclosed by the XPS depth profile. Hence, the XPS system is a very useful instrument to study the sputter effect on thin-film materials. Monoatomic Ar^+ and argon gas cluster ion beams (GCIBs), inert gases that have a low reaction with the material surface, are very common ion-beam sources for sputtering.[3,4] Before depth profiling is performed, a suitable

sputtering source should be selected to obtain accurate depth information. The monatomic Ar^+ ion beam is a basic sputtering source equipped with a surface analysis instrument, such as XPS, Auger electron spectroscopy, and time-of-flight secondary-ion mass spectrometry (ToF-SIMS), showing excellent sputter capability on metal and inorganic nanomaterials without contamination concerns. However, for some sensitive materials, the chemical state of the elements may be altered because of monatomic Ar^+ depth profiling.[5] For instance, the
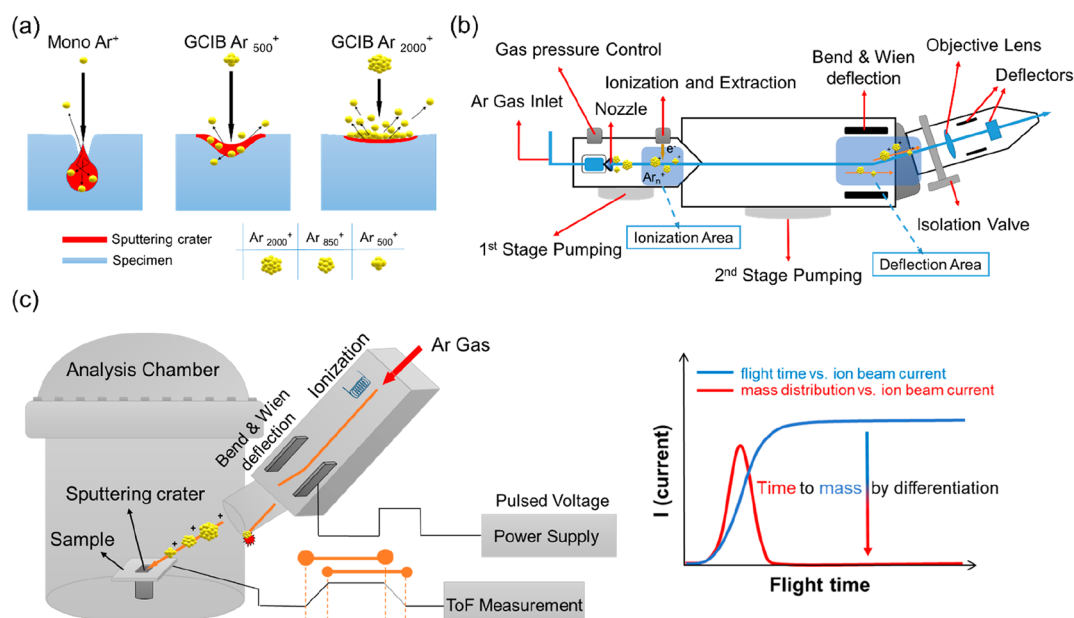
Figure 1. (a) Impact depth of sputtering with various ion cluster sizes. (b) Schematic of the Ar-GCIB ion source. (c) Ar-GCIB cluster size measurement on the XPS system.

preferential sputtering of O is a well-known phenomenon during depth profiling materials in the front-end fabrication process of semiconductor industries, such as TiO_2 and Ta_2O_5.[6,7] This concern could be worse if monatomic Ar^+ was used for detecting organic-based specimens. Preferential sputtering has been reported to cause damage to poly(ethylene terephthalate) (PET) and poly(tetrafluoroethylene) (PTFE) films.[8] The sputter damage was due to graphitization of the PET surface and fluorine evolution from PTFE. Hence, the monatomic Ar^+ source is not suitable for the sputtering of organic materials if information on the chemical state and quantification of the layer structure is required. For depth profiling of organics, GCIB is an alternative to reducing sputter damage of the nanoscale thin films.[9] The essential factor for selecting a suitable ion-beam source is scientifically based on the energy distributed on each atom. The effect of the energy per atom of cluster ion beams on depth profiling has been discussed in the last 5 years.[10,11] The sputter damage depth is known to be smaller when the low energy per atom of GCIB is used because the impact region of bombardment is shallower.[12] Hence, at a fixed beam energy, a large cluster size has a shallower impact depth than a small cluster size (Figure 1a). Moreover, the damage caused by sputtering is summarized as able to be suppressed if the energy per atom is smaller than the energy of the molecular bond dissociation in materials. The energy per atom of monatomic Ar^+ is usually higher than 500 eV; a beam energy range of 500 eV to 4 keV is commonly used. With a tunable cluster size, it is possible that the GCIB could provide a wider range of energy distributions on each atom. The energy per atom could even decrease to 2.5 eV/atom with a cluster size greater than 2000.[13] Hence, the larger size of the cluster ion beam is very useful for the sputtering of polymer materials with weak bond dissociation energies, such as C−C and C−O bonds, which are typically ∼3−5 eV.[14] As a result, a tunable GCIB has become one of the most promising techniques to preserve the chemical structure of organics during the sputtering of nanoscale thin films. In addition, the sputter damage caused by monatomic Ar^+ has

been reported to be able to even be removed using a large-cluster GCIB.[15,16] However, GCIB with a large cluster size could be utilized to reduce the sputter damage to inorganic materials, such as metal oxides. The sputter rate was found to decrease with a smaller energy per atom. A sputter-induced surface roughness was also reported to be increased with a smaller energy per atom of GCIB on inorganic materials,[17] which may be attributed to the low sputter rate on inorganic materials, resulting in the accumulation of damage during depth profiling, which showed the opposite trend: the roughness of the sputtering on organics was increased with a larger energy per atom of GCIB.[4] However, GCIBs with large cluster sizes have difficulty providing practical sputter rates for metal/inorganic-related semiconductor devices. Nevertheless, multiple and diverse hybrid materials are commonly introduced in 5G telecommunications chips and displays, such as front-end, middle-end, and back-end fabrication processes of semiconductor devices and other next-generation organic electronics.[18,19]

The architecture of the devices often consists of multiple metal/organic/inorganic layers. When information on both organics and inorganics is required to be collected in these hybrid nanomaterials, neither monatomic Ar^+ nor a GCIB with a large cluster size could provide it because of the sputter damage to organics and a very low sputter rate on metals/inorganics, respectively. Recently, because of the property of the tunable energy per atom of GCIB, a small-cluster GCIB may still be considered to hold the capability of low sputter damage to organics. while the sputter yield on metals/inorganics may be enhanced because the energy per atom was increased. A small-cluster GCIB was then applied to the depth profiling of the hybrid samples.[20] Ar_{500}^+, with an energy per atom of 16 eV, has been reported to show good capability for the depth profiling of perovskite hybrid devices with less fragmentation of the organic layer. Although the sputtering was less efficient than that of monatomic Ar^+, the required sputter time for removing the top metal layer of the device was within 1 h in the ToF-SIMS depth profile. Increasing the energy per

atom could attenuate the sputter inefficiency by using a smaller cluster size or higher beam energy. Hence, the selection of the cluster size of GCIB has been known to play an important role in sputtering a wider range of hybrid materials on the nanometer scale. To determine an optimized beam condition, a test on the depth profiling of each component in hybrid samples is necessary. To explore more GCIB cluster size selection for depth-profiling applications, a GCIB cluster size measurement tool has been developed and installed on the XPS system in this work. The measurement of the actual cluster size distribution was realized in the XPS system. The systematic check of the GCIB cluster size distribution and its effect on the sputtering behavior was also investigated, including the sputter rate and sputter damage. GCIB settings with a series of cluster sizes were applied to depth profiling on inorganic, organic, and hybrid samples. The practical application of a GCIB with a tunable cluster size on depth profiling will be discussed.

2. RESULTS AND DISCUSSION

2.1. Measurement of the Ar-GCIB Cluster Size. In a conventional XPS instrument, there is no tool for measuring the GCIB cluster size. The parameters of the GCIB are given by factory settings. Hence, the actual cluster size distribution cannot be examined if the parameter is changed. Users are also limited in setting up other GCIB parameters to obtain different cluster sizes because several parameters affect the cluster size distribution, including the argon gas pressure, ionization energy, beam energy, extractor voltage, and the setting of the condenser lens. To realize measurement of the cluster size distribution on the XPS system, a cluster size measurement tool has been developed and installed on a PHI VersaProbe III XPS system, which is already equipped with a GCIB option (Figure 1). The cluster size is measured using a time-of-flight mass separation method.[21] After Ar_n^+ ions are extracted, the cluster ion beam is deflected to eliminate neutral species and monomer through bending and a magnetic Wien filter, respectively, before focusing and sputtering the samples, as shown in Figure 1b. A rise-up beam is generated by giving a pulsed voltage to bend the ion beam, which provides the flight-starting time, as shown schematically in Figure 1c. The current profile is recorded from the flight-starting time until the largest mass ions arrive at the sample. The cluster size distribution is obtained by converting the flight time to mass. In our experience, the argon gas pressure and beam energy are dominant parameters that change the cluster size distribution. In this work, the tuning of each GCIB setting is executed after a set value of the argon gas pressure is reached and stable. The beam energy is fixed at 20 kV in all GCIB settings, so naturally the energy per atom is higher with a smaller cluster size. Then, all ion-beam parameters, including the settings of the extractor, condenser lens, objective lens, and bend and Wien deflection, are optimized to obtain a focused beam with a maximum target current. A series of GCIB peak cluster sizes—Ar_{2000}^+, Ar_{1200}^+, Ar_{850}^+, Ar_{600}^+ and Ar_{500}^+—is made, and the beam target currents for each setting are listed in Table 1. The cluster distributions of each Ar_n^+ are shown in Figure 2. The energy per atom values for each GCIB setting are calculated with the beam energy divided by the number of peak cluster sizes and are listed in Table 1. The sputter rate of the material is known to be dependent on the current and energy per atom of the GCIB, and a larger current or higher energy per atom increases the efficiency of sputtering. However, a smaller argon gas

Table 1. Ar-GCIB Settings with a Series of Cluster Numbers and Measured Sputter Rates on SiO_2, NiO_x, and TiO_2[a]

ion beam	Ar-GCIB					Ar⁺
cluster size	2000	1200	850	600	500	1
beam voltage (kV)	20	20	20	20	20	1
target current (nA)	50	33	15	10	3	680
beam current density ($\mu A/cm^2$)	67.26	44.84	16.10	11.62	5.91	326.11
energy per atom (eV)	10	17	24	33	40	1000
sputter raster size (mm^2)	1					
sputter rate on SiO_2 (nm/min)	10.20	7.04	5.95	6.41	3.53	6.30
normal sputter rate on SiO_2 (nm/min × nA)	0.20	0.21	0.40	0.64	1.18	0.01
sputter rate on NiO_x (nm/min)	7.00	5.72	3.40	3.76	2.36	7.50
normal sputter rate on NiO_x (nm/min × nA)	0.14	0.17	0.23	0.38	0.79	0.01
sputter rate on TiO_2 (nm/min)	0.28	4.00	2.60	1.58	0.64	7.80
normal sputter rate on TiO_2 (nm/min × nA)	0.01	0.12	0.17	0.16	0.21	0.01

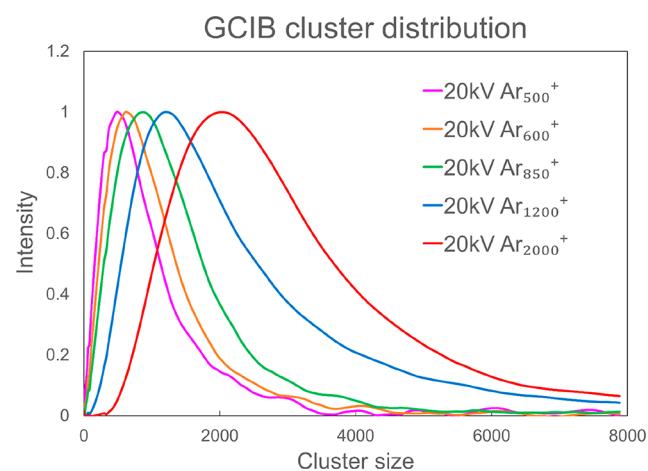[a]The raster size of each depth profiling is 1 mm^2.

Figure 2. Cluster size distribution of GCIB Ar_n^+ settings.

pressure is used to obtain a smaller cluster size with higher energy per atom, resulting in a lower target current of the GCIB. Hence, both the target current and energy per atom are listed in Table 1 for comparison. In conclusion, the results show that cluster size measurement of the customized GCIB parameters on the XPS system is realized and can be executed any time before XPS depth profiling is performed.

2.2. Sputter Rate and Damage Conditions on Inorganics. The sputter rate of each GCIB setting on a standard SiO_2 thin film was measured (Table 1). The current density is known to be one of the critical factors affecting the sputter rate of the ion beam. To estimate the effect of different cluster sizes on the sputtering of SiO_2, the sputter rate is normalized to the target current. The normalized sputter rate increases with a smaller cluster size, which is consistent with the statements above. Table 1 also lists the sputtering behaviors of each GCIB cluster size on NiO_x and crystal TiO_2 thin films, which have been widely adopted in the field of

semiconductor analysis. The normalized sputter rates on NiO_x and crystal TiO_2 show consistent results with the SiO_2 specimen, which is shown in Figure 3. The smaller the cluster
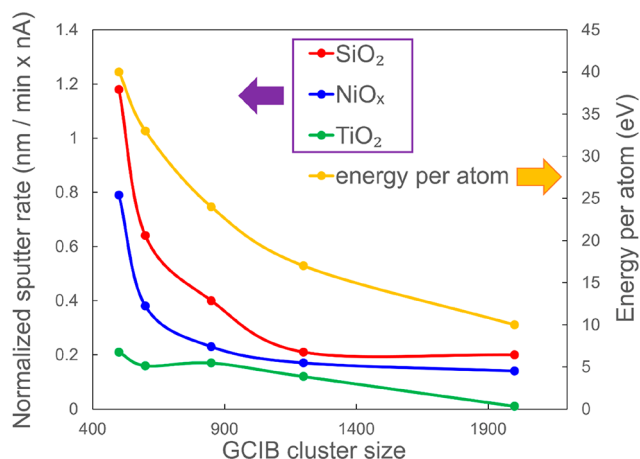

Figure 3. Normalized sputter rates versus cluster sizes for SiO_2, NiO_x, and TiO_2.

size, the higher the sputter rate obtained. With increased energy per atom of smaller cluster size, the curve of the sputter yield as a function of the cluster size (Figure 3) is found to have a trend similar to that in the literature.[22] Figure 3 also shows the rapid growth of the sputter rate in SiO_2 when the cluster size is tuned from 850 to 500, possibly attributable to the energy on each cluster atom surpassing the sputter threshold energy of the material.[23] Similar phenomena are also observed in NiO_x. The depth profiling of a TiO_2 film using a smaller-cluster GCIB does not show significant growth in the sputter rate, and further investigation on the sputter threshold energy of TiO_2 is required.

The chemical state is another concern during sputtering. The chemical state of certain metal oxides is usually altered (reduced) by Ar^+ ion sputtering, which results in unreliable chemical state information. The damage conditions of GCIB with a series of cluster sizes are examined. High-resolution XPS spectra of NiO_x and TiO_2 were acquired to investigate the chemical state change after sputtering using monatomic Ar^+ or GCIBs. The spectra at the same sputter depth are extracted for comparison. Figure 4a shows that a reduction of the Ni 2p peaks is observed either with sputtering of monatomic Ar^+ or with GCIB of various cluster sizes. When a smaller cluster size

is chosen, the ratios of Ni^0 to Ni^{2+} and Ni^{3+} increase, suggesting that a more severe reduction in Ni 2p occurs when a smaller cluster size is used for sputtering. However, the reduction level is still less than the result of monatomic Ar^+ sputtering. The chemical state variation of the O 1s spectra is also examined, and the variation is found to be similar in the depth profiles with any GCIB cluster size used in this work. The O 1s spectra extracted from GCIB Ar_{500}^+ are used here to present the chemical state variation (Figure 4b). The spectrum of the surface before sputtering shows the typical O 1s chemical state of a nonsintered NiO_x film,[24] and the O 1s peaks of NiO (529.89 eV) and NiOOH (531.61 eV) are detected. After sputtering, the ratio of NiOOH to NiO decreases, suggesting that preferential sputtering of O occurs. The decrease in the O atomic concentration during sputtering can be observed in Figure S1. Similar reduction phenomena are also observed in TiO_2 depth profiling (Figure 4c). The ratios of Ti^0, Ti^{2+}, and Ti^{3+} to Ti^{4+} increased with sputtering of a smaller cluster size. The reduction level increases with sputtering using a smaller cluster size, but GCIB still has the advantage of preserving the chemical state of TiO_2 over monatomic Ar^+, as reported.[25] The O atomic concentration in the TiO_2 depth profile of Ar_{500}^+ shows no significant change because the reduction to Ti^0 metal is rather low compared to the reduction to Ti^{2+} and Ti^{3+} oxides (Figure S1). A slow decrease in O 1s in the TiO_2 depth profile of monatomic Ar^+ is observed, suggesting the preferential sputtering of O. Hence, compared to monatomic Ar^+, GCIB sputtering illustrates fewer reduction phenomena in both the Ni 2p and Ti 2p spectra. Moreover, sputtering using a smaller-cluster GCIB causes more chemical reduction, which could result in misleading information. In other words, the chemical damage is gradually reduced with increasing GCIB cluster size. In summary, the results suggest that the sputter rate on inorganics could be enhanced with a smaller GCIB cluster size. The chemical damage to sputter-sensitive inorganic materials is alleviated with a larger GCIB cluster size but at the cost of a reduced sputter rate.

2.3. Sputter Rate and Damage Conditions to Organics.

A large argon cluster ion beam is known for its relatively high sputter rate with low damage to organics. With regard to a smaller cluster size, the sputtering impact on organics needs to be considered because the elemental distribution and chemical state could be disturbed, similar to the behavior using monatomic ion beams. PET, poly(methyl methacrylate) (PMMA), and polyimide (PI) are widely used
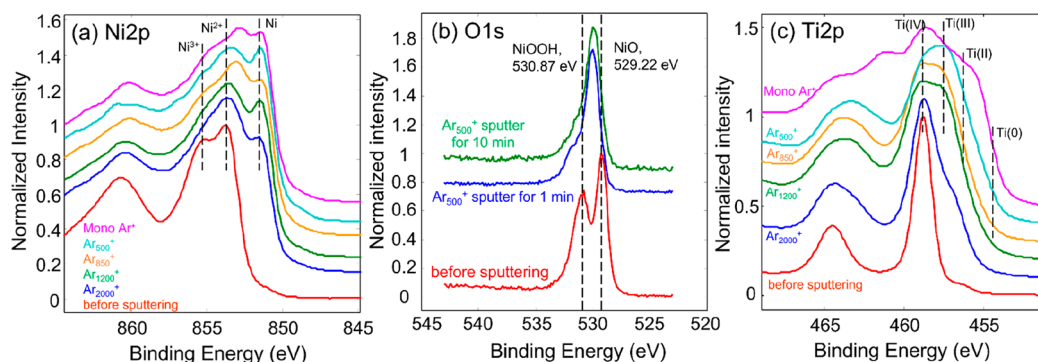

Figure 4. XPS spectra of (a) Ni 2p, (b) O 1s of nickel oxide, and (c) Ti 2p of TiO_2 before and after GCIB or monatomic Ar sputtering. The sputter depth of each GCIB is ~10 nm in parts a and c.
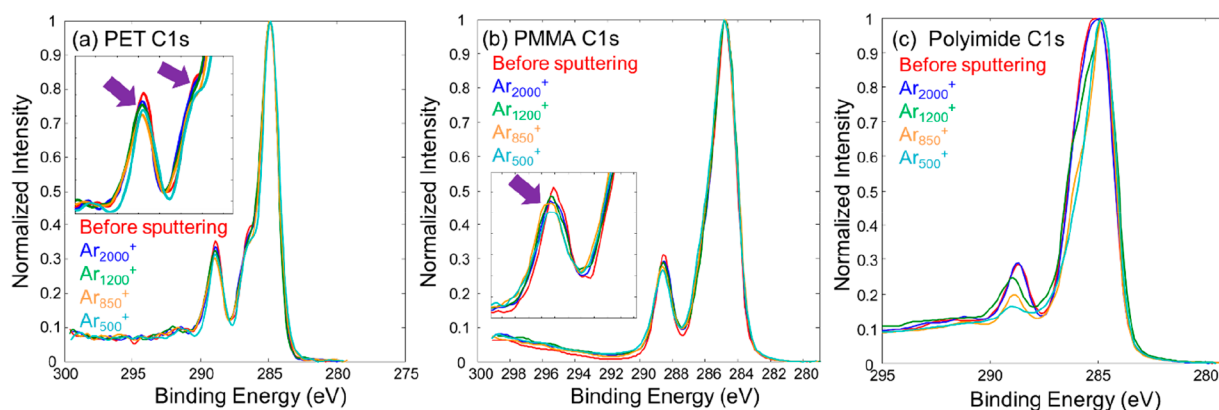
Figure 5. XPS C 1s spectra of (a) PET, (b) PMMA, and (c) PI before and after GCIB sputtering.

polymers for IC packaging in far back-end processes. In this study, these three polymers were selected to investigate the difference in the chemical state before and after 10 min of sputtering. Figure 5a shows that, compared to monatomic Ar^+ sputtering,[26] GCIB sputtering causes less damage to PET films. However, minor sputter damage could still be observed. The ratio of −CO and −COO groups to hydrocarbons was found to be lower, with smaller cluster GCIB sputtering in general (purple arrows). This result suggested that sputter damage on the PET film was increased with a smaller cluster size. In general, the sputter yield (normalized sputter rate in the paper) increased with smaller cluster size (higher energy per atom), Ar_{500}^+ may remove the surface damage caused by sputtering faster than Ar_{850}^+. Therefore, a more undamaged surface (newly exposed surface) could be detected, which results in a higher −COO ratio in Figure 5a. Although the XPS spectral shapes show no dramatic change with the energy per atom up to 40 eV, the sputter rate at PET had been reported to decrease in the ToF-SIMS depth profile when a GCIB with an energy per atom of 20 eV is used.[4] Ion-induced cross-linking and carbonization led to suppression of the sputter rate and ion intensity. Compared to the ToF-SIMS depth profile, a longer sputter depth may be required to observe more accumulation of sputter damage with obvious changes in the XPS spectrum.

In the spectra of PMMA (Figure 5b), the ratio of −COO groups to hydrocarbons also slightly decreased with a small cluster size. The results also suggested that sputter damage was enhanced with a small cluster size. Therefore, from the change in the spectral shape in PET and PMMA, the data suggest that differential sputtering between O and C was enhanced with a small cluster size. PI compounds have been used in diverse applications because of their high heat resistance. However, sputter damage using monatomic Ar^+ is commonly observed,[15,27] which results in errant chemical state information. Moreover, sputter damage using a GCIB with a high beam voltage was also reported. Hence, depth profiling using GCIB with known cluster sizes was then performed. Figure 5c reveals that the C 1s spectra of PI significantly changed when the GCIB cluster size was below 2000. Even though the energy per atom of Ar_{1200}^+ was as low as ∼17 eV, it still caused sputter damage to PI. Differential sputtering among N, O, and C nuclei was observed. Therefore, a high-resolution XPS spectrum was shown to be necessary to comprehensively find a suitable GCIB cluster size for sputter-sensitive organics.

2.4. Depth Profiling in a Hybrid Sample. The depth profiling of inorganic/organic hybrid devices has been reported to be difficult because it is difficult to find a balance between the practical measurement cycle time and the preservation of chemical information. When depth profiles were performed from both sides of a perovskite, sputter artifacts from the bombardment of primary ion and sputter ion beams (Bi^+, Bi_3^+, O_2^+, and $Ar_{500-3000}^+$) in ToF-SIMS analysis were reported to be observed.[28−30] While monatomic ion-beam sputtering causes severe damage to organics, large-cluster GCIBs have difficulty removing metal layers from hybrid materials. Therefore, GCIB with a small cluster size was used to perform depth profiling on the hybrid sample because the energy per atom is increased to enhance the sputter rate and the cluster property holds the capability of low sputter damage to organics. In this work, depth profiling using GCIB with a specific cluster size was performed. The device architecture of a perovskite solar cell is shown in Figure 6a. It was difficult to examine the sputter damage of the phenyl-C61-butyric acid methyl ester (PCBM) layer in the XPS system because the chemical bonds are composed mainly of C−C/C−H bonds (Figure 6b). Hence, the fragmentation of PCBM was analyzed using ToF-SIMS. The sputtering behavior of monatomic ion beams and Ar_{1500}^+ (5 keV, ∼3 eV/atom) on PCBM was reported.[31] Therefore, ToF-SIMS depth profiling using Ar_{2000}^+ (∼10 eV/atom) and Ar_{600}^+ (∼33 eV/atom) was performed here to examine the sputter damage of a PCBM thin film on an indium−tin oxide (ITO) substrate. The substrate effect of PCBM deposition on ITO glass is also taken into consideration based on previous experience. The similar thickness of PCBM could be controlled with a suitable ITO pretreatment compared to the conventional PCBM deposition on perovskite thin films. The molecular integrity of PCBM was maintained after Ar_{2000}^+ or Ar_{600}^+ sputtering without a significant decrease in the $[C_{60}]^+$ intensity (Figure 6c). Figure 7a shows the XPS depth profile of the perovskite device using Ar_{2000}^+ as the sputtering source. The sputter rate on metal (Ag) is observed to be quite low, and the layer structure is ill-defined. The metallic cathode layer could not be removed efficiently, and the layer structures contained no interfacial information. Depth profiling on hybrid samples with large cluster sizes has been reported to cause obvious differential sputtering effects.[32] It is then suggested to choose a smaller-cluster Ar_{600}^+ ion beam for further device examination. Selection of Ar_{600}^+ instead of Ar_{500}^+ is due to the higher beam target current of Ar_{600}^+. In general, a higher beam current
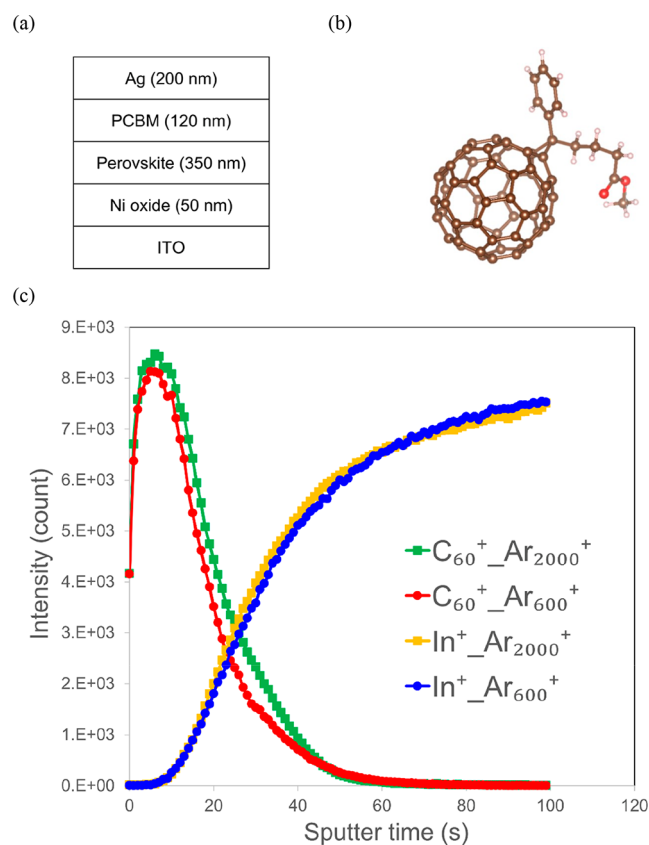
E

Figure 6. (a) Layer structure of the perovskite device, (b) PCBM chemical structure, and (c) ToF-SIMS depth profile of the PCBM thin film on the ITO substrate. The energy of each GCIB is fixed at 20 kV.

shows a higher sputter rate. Although Ar_{500}^+ also shows a higher normalized sputter rate (sputter yield), it can be found that its sputter rate is lower than those of other cluster sizes, which leads to a longer acquisition time for the complete depth profile for inorganic layers. It is also observed that Ar_{2000}^+ shows a low sputter rate to the metal layer. On the basis of the above conditions, Ar_{600}^+ is selected for depth profiling of perovskite devices. The XPS depth profile using the Ar_{600}^+ ion beam is illustrated in Figure 7b, where the layer structure of the perovskite solar cell can be observed to have been preserved. Compared to the depth profile using Ar_{2000}^+, the metallic layer

could be removed by using Ar_{600}^+ with obvious interface information. The low detection of N 1s and I 3d5 from the perovskite layer is caused by degradation.[33] A reduction in NiO_x can be observed, which illustrates a similar Ni metallic peak at ~852.5 eV, as shown in Figure 4a, and the reduction level increases with the sputter time. The Ni 2p spectrum extracted from the interface of the perovskite device is shown in Figure S2. Metal Pb^0 was also observed as expected, and Pb^0 existed in the process of sample preparation. No sputter damage accumulation was reported with Ar_{75}^+ and Ar_{500}^+ sputtering.[20] C was detected in the Ag layer, and the Ag layer accumulated in deeper layers, coming from the common phenomenon of perovskite degradation.[34,35] However, compared to the depth profile of monatomic Ar^+ (Figure 7c), Ag accumulation between the perovskite and NiO_x layer is approximately twice as high in the depth profile of GCIB Ar_{600}^+ and has a long tail into the NiO_x layer, suggesting the low sputter rate of GCIB at the metal. Pb and I tailing into the ITO layer was observed in the depth profile of GCIB sputtered with 20 kV Ar_{4000}^+ but was suppressed when 20 kV Ar_{1000}^+ was used.[36] Although this phenomenon could not be examined because of the ill-defined layer due to the metal layer when Ar_{2000}^+ was used, the Ar_{600}^+ result showed no increased Pb and I tailing into the NiO_x layer, which is similar to the depth profile of monatomic Ar^+. Nevertheless, although the sputter efficiency was less than monatomic Ar^+, as reported,[20] the layer sequence was clearly obtained in the depth profile of Ar_{600}^+. For the sputter rate difference among each of the layers, the sputter rate on each layer was calculated using the thickness in Figure 6a. The sputter rate in the organic layer (~10.4 nm/min) was higher than the sputter rate in the metal Ag (~5.6 nm/min) and NiO_x layers (~2.2 nm/min). These results show that GCIB with a small cluster size still shows a higher sputter efficiency for organic materials than inorganics and metals. However, compared to GCIB Ar_{2000}^+, the sputter rate difference between organic and metal/inorganic materials is obviously smaller.

3. CONCLUSIONS

The sputtering behavior of GCIB has been reported to be adjustable using different cluster sizes. In this work, an XPS system equipped with a cluster size measurement kit was developed. The actual cluster size was measured using the ToF method for any GCIB setting. Hence, by tuning of the ion gun and measurement of the cluster size distribution, GCIB
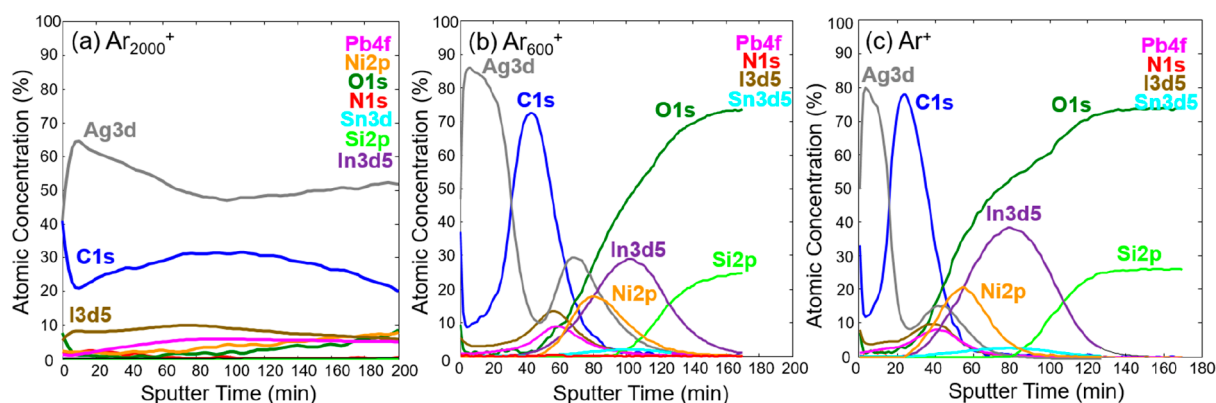

Figure 7. XPS depth profile of the perovskite device using GCIB: (a) Ar_{2000}^+; (b) Ar_{600}^+; (C) monatomic Ar^+. The cluster energy is 20 kV for each GCIB and 1 kV for monatomic Ar.

settings with specific cluster size and energy per atom could be obtained before XPS analysis. GCIB $Ar_{500-2000}^+$ ion beams were made and used for depth profiling on various nanomaterials, and the results of the depth profiles were similar to the results reported. Depth profiling using different cluster sizes on SiO_2, NiO_x, and TiO_2 showed that the sputter rate on inorganics could be enhanced with smaller cluster sizes and sputter damage is observed. However, the chemical state change of sputter-sensitive inorganics using GCIB could be reduced compared to monatomic Ar^+ sputtering. Additionally, three different polymers were used to investigate the chemical state change with different cluster sizes. Sputter damage was observed in PET, PMMA, and PI, leading to a correlation between the sputter damage and energy per atom. However, the differential sputtering on PET and PMMA is less than that on PI. We concluded that the sputter damage varies with the material. Moreover, depth profiling of hybrid samples using small-cluster GCIB was also examined. The depth profile of a perovskite device showed that using a small-cluster GCIB could deliver a reasonable sputter rate on a hybrid sample with a metal/organic/inorganic structure.

In conclusion, the development of a GCIB cluster size measurement kit on an XPS system accesses GCIB cluster size measurements for any customized parameters. The actual cluster size distribution is available before XPS depth profiling. This cluster size measurement kit could become a useful tool in the investigation of optimized GCIB settings for balancing the sputter damage and sputter rate for novel nanomaterials and complicated hybrid samples.

4. EXPERIMENTAL SECTION

GCIB Cluster Size Measurement. ToF mass measurement is commonly used in high-resolution mass spectrometry, and a mass can be obtained by converting the flight time into ion mass with conditional parameters of kinetic energy, flight distance, etc. The GCIB cluster size measurement tool (PHI MOD1310) on an ULVAC-PHI VersaProbe III system was developed. In the ULVAC-PHI GCIB system (PHI MOD06-2500 and MOD06-2500A) installed on the 65° incident port of VersaProbe III, a ToF mass separation of the rising-up step-pulsed method was applied to measure the cluster size (Figure 1). When a pulsed voltage was given to bend the ion beam, a beam rise-up was generated and gave the flight-starting time. This beam rise-up gave a sufficiently short time at the flight-starting time, and the beam current profile was continually measured at the detector from the starting time until the largest mass ions certainly arrived at the detector. Through differentiation of the current profile with respect to the flight time, the mass distribution of the ion beam could be obtained. The gas pressure and beam voltage are two of the main factors that affect the cluster size distribution and beam current density. The beam voltage was fixed at 20 kV, and the gas pressure in the range from 450 to 650 kPa was adjusted to obtain a cluster size distribution from 500 to 2000. The extractor, bend, and Wien deflections were tuned to gain the maximum beam current measured on the sample holder (SUS304 stainless steel) at an incident angle of 65°. Then, Ar-GCIB was focused by tuning the objective lens. All parameters of these Ar-GCIB settings were repeatedly tuned to obtain the desired cluster size distribution before depth profiling was performed. The peak cluster size was used to present the cluster size of each Ar-GCIB setting. The sputter rate of these Ar-GCIB settings was calibrated using a known thickness from the material manufacturer or measured using a step profilometer (DEKTAK 6M, Bruker, Germany).

Sample Preparation. Standard samples used in this work included PET, PMMA, PI, and crystal TiO_2. The PSC devices were glass/ITO/NiO_x/$MAPbI_3$/$PC_{61}BM$/Ag and were fabricated as follows. ITO-coated glass substrates (15 Ω/cm^2) were ultrasonically

cleaned in detergents, deionized water, acetone, and isopropyl alcohol for 15 min each and subsequently dried in a N_2 gas flow. NiO_x films were spin-coated onto the ITO layer from 70 μL of a 0.3 M nickel 2-ethylhexanoate solution in ethanol at 1700 rpm for 35 s. The samples were heated from 70 °C and then increased to 20 °C every 5 min until 300 °C was reached following 1 h of annealing. A solution of PbI_2 (460 mg/mL) was dissolved in N,N-dimethylformamide, heated to 70 °C while being continuously stirred, deposited on top of the NiO_x layer by spin coating at 6000 rpm for 30 s, and then annealed at 70 °C for 10 min. Then, the samples were dipped into a solution of CH_3NH_3I dissolved in 2-propanol (40 mg/mL) at 3000 rpm for 60 s and annealed at 100 °C for 20 min. The $PC_{61}BM$ layer was spin-coated from a toluene solution of 20 mg/mL at 1000 rpm for 30 s. $MAPbI_3$ and $PC_{61}BM$ were all spin-coated under ambient conditions. Finally, an Ag film with a thickness of approximately 200 nm was deposited onto the $PC_{61}BM$ layer by using a thermal evaporation process. For a 50 nm nickel oxide thin film on an ITO-coated glass slide, the preparation method was the same as that for the NiO_x layer in the PSC devices.

XPS and ToF-SIMS Depth Profiling. All XPS depth profiling was performed with a PHI VersaProbe III (ULVAC-PHI, Inc., Japan) XPS system. The chemical state of the materials was analyzed using microfocused Al K_α X-rays (25 W, 15 kV), and dual-beam charge neutralization (a 1 V electron beam and a 7 V Ar^+ ion beam) was applied during analysis. For the sputter phase, a 1 kV monatomic Ar^+ ion beam and a 20 kV GCIB with a specific cluster size were used. The sputter raster size was set to 1 mm × 1 mm. To calculate the sputter rate, the sputter crater was measured using a stylus profiler (DEKTAK 6M, Germany). An average sputter depth of 0.5 mm × 0.5 mm area from the center position of the crater was recorded. The sputter rate was obtained by dividing the sputter depth by the total sputter time.

ToF-SIMS depth profiling on a $PC_{61}BM$ thin film was performed with a PHI nanoTOF II instrument (ULVAC-PHI, Inc., Japan). The $PC_{61}BM$ layer was spin-coated on ITO glass from a toluene solution of 20 mg/mL concentration at 2000 rpm for 30 s. Bi_3^{+2} (30 kV) was used to probe the $PC_{61}BM$ surface in the analysis phase with a raster size of 100 μm × 100 μm. GCIB Ar_{2000}^+ and Ar_{600}^+ (20 kV) were used in the sputter phase with raster sizes of 2000 μm × 2000 μm. The sputter interval was set to 1 s. No neutralization was applied during the analysis or sputter phase.

■ ASSOCIATED CONTENT

Ⓢ Supporting Information

The Supporting Information is available free of charge at https://pubs.acs.org/doi/10.1021/acsanm.2c00202.

Figure S1 illustrating the depth profiles overlay of NiO_x (Ar_{500}^+) and TiO_2 (Ar_{500}^+ and monatomic Ar^+) and Figure S2 demonstrating the Ni 2p spectrum extracted from the interface of perovskite and the NiO_x layer (PDF)

■ AUTHOR INFORMATION

Corresponding Authors

Wei-Chun Lin − *Department of Photonics, National Sun Yat-Sen University, Kaohsiung City 804, Taiwan;* ⓞ orcid.org/0000-0001-5722-6383; Email: wclin@mail.nsysu.edu.tw

Takuya Miyayama − *Analytical Laboratory, ULVAC-PHI, Inc., Chigasaki, Kanagawa 253-8522, Japan;* Email: takuya_miyayama@ulvac.com

Authors

Hsun-Yun Chang − *Analytical Laboratory, ULVAC-PHI, Inc., Chigasaki, Kanagawa 253-8522, Japan*

Po-Chih Chu − *Department of Photonics, National Sun Yat-Sen University, Kaohsiung City 804, Taiwan*

Yi-Kai Wang − *Department of Photonics, National Sun Yat-Sen University, Kaohsiung City 804, Taiwan*

Mauo Sogo − *Analytical Laboratory, ULVAC-PHI, Inc., Chigasaki, Kanagawa 253-8522, Japan*

Shin-ichi Iida − *Analytical Laboratory, ULVAC-PHI, Inc., Chigasaki, Kanagawa 253-8522, Japan*

Chien-Jung Peng − *Analytical Laboratory, ULVAC-PHI, Inc., Chigasaki, Kanagawa 253-8522, Japan*

Complete contact information is available at:
https://pubs.acs.org/10.1021/acsanm.2c00202

Author Contributions

†These authors contributed equally to this work.

Notes

The authors declare no competing financial interest.

REFERENCES

(1) Briggs, D. X-Ray Photoelectron Spectroscopy (XPS). *Handbook of Adhesion: Second Edition* **2005**, 621.

(2) Martin, P. M. *Handbook of Deposition Technologies for Films and Coatings*; Elsevier, 2010 ; pp 727−725.

(3) Liao, H. Y.; Tsai, M. H.; Kao, W. L.; Kuo, D. Y.; Shyue, J. J. Effects of the Temperature and Beam Parameters on Depth Profiles in X-Ray Photoelectron Spectrometry and Secondary Ion Mass Spectrometry under C60+-Ar+ Cosputtering. *Anal. Chim. Acta* **2014**, *852*, 129.

(4) Wang, S. K.; Chang, H. Y.; Chu, Y. H.; Kao, W. L.; Wu, C. Y.; Lee, Y. W.; You, Y. W.; Chu, K. J.; Hung, S. H.; Shyue, J. J. Effect of Energy per Atom (E/n) on the Ar Gas Cluster Ion Beam (Ar-GCIB) and O2+ Cosputter Process. *Analyst* **2019**, *144*, 3323.

(5) Lin, Y. C.; Chen, Y. Y.; Yu, B. Y.; Lin, W. C.; Kuo, C. H.; Shyue, J. J. Sputter-Induced Chemical Transformation in Oxoanions by Combination of C60+ and Ar+ Ion Beams Analyzed with X-Ray Photoelectron Spectrometry. *Analyst* **2009**, *134*, 945.

(6) Counsell, J. D. P.; Roberts, A. J.; Boxford, W.; Moffitt, C.; Takahashi, K. Reduced Preferential Sputtering of TiO2 Using Massive Argon Clusters. *J. Surf. Anal.* **2014**, *20*, 211.

(7) Simpson, R.; White, R. G.; Watts, J. F.; Baker, M. A. XPS Investigation of Monatomic and Cluster Argon Ion Sputtering of Tantalum Pentoxide. *Appl. Surf. Sci.* **2017**, *405*, 79.

(8) Yancey, D. F.; Reinhardt, C. Damage and Repair of Organic and Inorganic Surfaces by Ar + Ion and Gas Cluster Ion Beam Sputtering. *J. Electron Spectrosc. Relat. Phenom.* **2019**, *231*, 104.

(9) Mahoney, C. M. *Cluster Secondary Ion Mass Spectrometry: Principles and Applications*; John Wiley and Sons Inc.: Hoboken, NJ, 2013.

(10) Yang, L.; Seah, M. P.; Gilmore, I. S. Sputtering Yields for Gold Using Argon Gas Cluster Ion Beams. *J. Phys. Chem. C* **2012**, *116*, 23735.

(11) Seah, M. P. Universal Equation for Argon Gas Cluster Sputtering Yields. *J. Phys. Chem. C* **2013**, *117*, 12622.

(12) Toyoda, N.; Yamada, I. Gas Cluster Ion Beam Equipment and Applications for Surface Processing. *IEEE Trans. Plasma Sci.* **2008**, *36*, 1471.

(13) Winograd, N. Gas Cluster Ion Beams for Secondary Ion Mass Spectrometry. *Annu. Rev. Anal. Chem.* **2018**, *11*, 29.

(14) Cumpson, P. J.; Portoles, J. F.; Barlow, A. J.; Sano, N. Accurate Argon Cluster-Ion Sputter Yields: Measured Yields and Effect of the Sputter Threshold in Practical Depth-Profiling by x-Ray Photoelectron Spectroscopy and Secondary Ion Mass Spectrometry. *J. Appl. Phys.* **2013**, *114*, 124313.

(15) Miyayama, T.; Sanada, N.; Bryan, S. R.; Hammond, J. S.; Suzuki, M. Removal of Ar+ Beam-Induced Damaged Layers from Polyimide Surfaces with Argon Gas Cluster Ion Beams. *Surf. Interface Anal.* **2010**, *42*, 1453.

(16) Iida, S.; Carr, D. M.; Fisher, G. L.; Miyayama, T. Accurate and Reproducible In-Depth Observation of Organic−Inorganic Hybrid Materials Using FIB-TOF-SIMS. *J. Vac. Sci. Technol. B, Nanotechnol. Microelectron. Mater. Process. Meas. Phenom.* **2018**, *36* (3), 03F107.

(17) Ellsworth, A. A.; Young, C. N.; Stickle, W. F.; Walker, A. V. New Horizons in Sputter Depth Profiling Inorganics with Giant Gas Cluster Sources: Niobium Oxide Thin Films. *Surf. Interface Anal.* **2017**, *49*, 991.

(18) Chiba, T.; Kumagai, D.; Udagawa, K.; Watanabe, Y.; Kido, J. Dual Mode OPV-OLED Device with Photovoltaic and Light-Emitting Functionalities. *Sci. Rep.* **2018**. DOI: 10.1038/s41598-018-29806-8.

(19) Chen, F. C. Emerging Organic and Organic/Inorganic Hybrid Photovoltaic Devices for Specialty Applications: Low-Level-Lighting Energy Conversion and Biomedical Treatment. *Advanced Optical Materials* **2019**, *7*, 1800662.

(20) Noël, C.; Pescetelli, S.; Agresti, A.; Franquet, A.; Spampinato, V.; Felten, A.; diCarlo, A.; Houssiau, L.; Busby, Y. Hybrid Perovskites Depth Profiling with Variable-Size Argon Clusters and Monatomic Ions Beams. *Materials (Basel)* **2019**, *12*, 726.

(21) Toyoda, N.; Saito, M.; Hagiwara, N.; Matsuo, J.; Yamada, I. Cluster Size Measurement of Large Ar Cluster Ions with Time of Flight. *Proceedings of the International Conference on Ion Implantation Technology* **1998**, 1234.

(22) Seki, T.; Murase, T.; Matsuo, J. Cluster Size Dependence of Sputtering Yield by Cluster Ion Beam Irradiation. *Nuclear Instruments and Methods in Physics Research, Section B: Beam Interactions with Materials and Atoms* **2006**, *242*, 179.

(23) Wu, S. M.; Van DeKruijs, R.; Zoethout, E.; Bijkerk, F. Sputtering Yields of Ru, Mo, and Si under Low Energy Ar+ Bombardment. *J. Appl. Phys.* **2009**, *106*, 054902.

(24) Hou, C. H.; Shyue, J. J.; Su, W. F.; Tsai, F. Y. Catalytic Metal-Induced Crystallization of Sol-Gel Metal Oxides for High-Efficiency Flexible Perovskite Solar Cells. *J. Mater. Chem. A* **2018**, *6*, 16450.

(25) Noël, C.; Pireaux, J.-J.; Busby, Y.; Agresti, A.; Pescetelli, S.; DiCarlo, A.; Houssiau, L. XPS Depth Profiles of Organo Lead Halide Layers and Full Perovskite Solar Cells by Variable-Size Argon Clusters. *Proceedings of the Conference on Physical Chemistry of Semiconductor Materials and Interfaces XVII*, San Diego, CA, 2018; SPIE, 2018.

(26) Holländer, A.; Haupt, M.; Oehr, C. On Depth Profiling of Polymers by Argon Ion Sputtering. *Plasma Processes and Polymers* **2007**, *4*, 773.

(27) Miyayama, T.; Sanada, N.; Suzuki, M.; Hammond, J. S.; Si, S.-Q. D.; Takahara, A. X-Ray Photoelectron Spectroscopy Study of Polyimide Thin Films with Ar Cluster Ion Depth Profiling. *J. Vac. Sci. Technol. A Vacuum, Surfaces, Film.* **2010**, *28*, L1.

(28) Harvey, S. P.; Zhang, F.; Palmstrom, A.; Luther, J. M.; Zhu, K.; Berry, J. J. Mitigating Measurement Artifacts in TOF-SIMS Analysis of Perovskite Solar Cells. *ACS Appl. Mater. Interfaces* **2019**, *11* (34), 30911.

(29) Harvey, S. P.; Li, Z.; Christians, J. A.; Zhu, K.; Luther, J. M.; Berry, J. J. Probing Perovskite Inhomogeneity beyond the Surface: TOF-SIMS Analysis of Halide Perovskite Photovoltaic Devices. *ACS Appl. Mater. Interfaces* **2018**, *10* (34), 28541.

(30) Harvey, S. P.; Messinger, J.; Zhu, K.; Luther, J. M.; Berry, J. J. Investigating the Effects of Chemical Gradients on Performance and Reliability within Perovskite Solar Cells with TOF-SIMS. *Adv. Energy Mater.* **2020**, *10*, 1903674.

(31) Smentkowski, V. S.; Zorn, G.; Misner, A.; Parthasarathy, G.; Couture, A.; Tallarek, E.; Hagenhoff, B. ToF-SIMS Depth Profiling of Organic Solar Cell Layers Using an Ar Cluster Ion Source. *J. Vac. Sci. Technol. A Vacuum, Surfaces, Film.* **2013**, *31*, 030601.

(32) Cumpson, P. J.; Portoles, J. F.; Barlow, A. J.; Sano, N.; Birch, M. Depth Profiling Organic/Inorganic Interfaces by Argon Gas Cluster Ion Beams: Sputter Yield Data for Biomaterials, in-Vitro
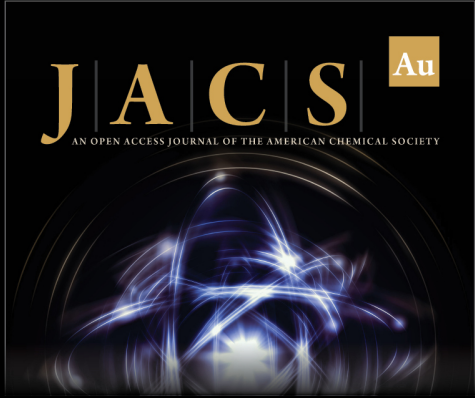
Diagnostic and Implant Applications. *Surf. Interface Anal.* **2013**, *45*, 1859.

(33) Lin, W. C.; Chang, H. Y.; Abbasi, K.; Shyue, J. J.; Burda, C. 3D In Situ ToF-SIMS Imaging of Perovskite Films under Controlled Humidity Environmental Conditions. *Adv. Mater. Interfaces* **2017**, *4*, 1600673.

(34) Ming, W.; Yang, D.; Li, T.; Zhang, L.; Du, M. H. Formation and Diffusion of Metal Impurities in Perovskite Solar Cell Material CH3NH3PbI3: Implications on Solar Cell Degradation and Choice of Electrode. *Adv. Sci.* **2018**, *5* (2), 1700662.

(35) Svanström, S.; Jacobsson, T. J.; Boschloo, G.; Johansson, E. M. J.; Rensmo, H.; Cappel, U. B. Degradation Mechanism of Silver Metal Deposited on Lead Halide Perovskites. *ACS Appl. Mater. Interfaces* **2020**, *12* (6), 7212.

(36) Hou, C. H.; Hung, S. H.; Jhang, L. J.; Chou, K. J.; Hu, Y. K.; Chou, P. T.; Su, W. F.; Tsai, F. Y.; Shieh, J.; Shyue, J. J. Validated Analysis of Component Distribution Inside Perovskite Solar Cells and Its Utility in Unveiling Factors of Device Performance and Degradation. *ACS Appl. Mater. Interfaces* **2020**, *12* (20), 22730.